Journal of Intelligent and Robotic Systems **1** (1988) 225–242.

Development of a Spherical Stepper Wrist Motor

KOK-MENG LEE
School of Mechanical Engineering, Georgia Institute of Technology, Atlanta, GA 30332, U.S.A

GEORGE VACHTSEVANOS
School of Electrical Engineering, Georgia Institute of Technology, Atlanta, GA 30332, U.S.A.

and

CHIKONG KWAN
School of Mechanical Engineering, Georgia Institute of Technology, Atlanta, GA 30332, U.S.A.

(Received: 15 March 1988)

Abstract. This paper presents the design concept of a new spherical stepper robotic wrist motor capable of three degrees of freedom (DOF) motion in a single joint. The spherical wrist motor has significant potential applications where the demands on wrist torque and workspace are low but high speed manipulation of end-effector orientation is required continuously in all directions. Typical applications are plasma and laser cutting and micro-assembly. The spherical motor is developed on the basis of the principle of variable reluctance stepper motors. This paper highlights the fundamental differences between the operation of a three DOF spherical motor and that of the conventional stepper motor. The establishment of a theoretic basis for design, prototype development and performance prediction is sought. In particular, an analysis of torque prediction is discussed along with the presentation of kinematic and dynamic relationships. A hybrid digital/analog laboratory prototype control circuitry has been developed to demonstrate proof of concept feasibility and to assist in achieving an optimum design.

Key words. Robotic wrist, spherical motor, and stepping motor.

1. Introduction

Recent developments in robotics, data driven manufacturing and high precision assembly have provided the motivation for the resurfacing of unusual designs of electro-mechanical transducers. A flurry of research activities is currently underway in direct drives involving DC, stepping, and brushless electro-mechanical actuators to improve performance by eliminating the problems inherent in the gear systems such as backlash, friction due to meshing, and mechanical compliance. These devices are normally employed to accomplish a single degree of motion manipulation at each joint [1–6]. An alternative design based on the concept of a spherical stepper wrist motor presents some attractive possibilities by combining pitch, roll, and yaw motion in a single joint. In addition to the compact design, the spherical wrist stepper motor results in relatively simple joint kinematics and has no singularities in the middle of the workspace except at the boundaries.

In some applications, such as high speed plasma and laser cutting, the demands on the workspace and the wrist force/torque requirements are low but the end effector is oriented quickly, continuously and isotropically in all directions. Unfortunately,

the popular three-consecutive-rotational-joints wrist possesses singularities within its workspace, which is a major problem in trajectory planning and control. At a singularity, the wrist cannot orient the end-effector in certain directions. Asada and Cro-Granlto [1] suggested relocation of the singularity outside the required workspace by varying the direction of the end-effector mount. Alternatively, the task may be rearranged such that the working space of the end-effector is not in the vicinity of the singularity [2]. However, in the vicinity of a singularity, the ratio of the rotation rate of the wrist joint to that of the end-effector is very large. Paul and Stevenson [2] defined the cone of degeneracy as the space in which the wrist-joint to end-effector rotation rate ratio is larger than twice the minimum in the entire workspace. In some cases, the cone of degeneracy can have a vertex angle of 60 degrees. In addition, significant undesired centrifugal effects are expected in the popular three-consecutive-rotational-joints wrist dynamics.

William *et al.* [7, 8] and Laithwaite [9] performed the original analysis on one form of spherical induction motor. Here, the application was in speed control for one-rotational axis–achieved by controlling the direction of the stator wave excitation at an arbitrary angle to the motor axis. Since the work in [7–9], little attention has been given to the spherical motor, with the exception to the design of a rotodynamic pump [10] and in gyroscope applications [11, 12]. A spherical induction motor was conceptualized in [13]. The authors presented a detailed analysis of the device based on a field theoretic concepts. This original development was suggested as a robotic wrist actuator in [6]. However, realization of a prototype spherical induction motor remains to be demonstrated. The mechanical design of a spherical induction motor is complex. Laminations are required to prevent movement of unwanted eddy currents. Complicated three phase windings must be mounted in recessed grooves in addition to the rolling supports for the rotor in a static configuration. These and other considerations lead to an investigation of an alternative spherical actuator based on the concept of variable reluctance (VR) stepper motor which is easier to manufacture. The trade-off, however, is that a sophisticated control scheme is required.

In this paper, the design concept of a spherical wrist motor based on the principle of variable reluctance (VR) stepper motor is presented. In particular, the paper highlights the fundamental differences between the principle of operation of the three DOF spherical motor and that of the conventional single-axis stepper motor. In addition, the torque and resolution predictions are discussed along with the presentation of kinematic and dynamical relationships. A laboratory prototype wrist and its associated hybrid digital/analog excitation and control circuitry have been developed to demonstrate proof of concept feasibility and to assist in achieving an optimum design.

2. Design Concepts

A schematic of a spherical stepper motor is shown in Figure 1. It must be pointed out that the device shown in the figure does not represent an optimum configuration.

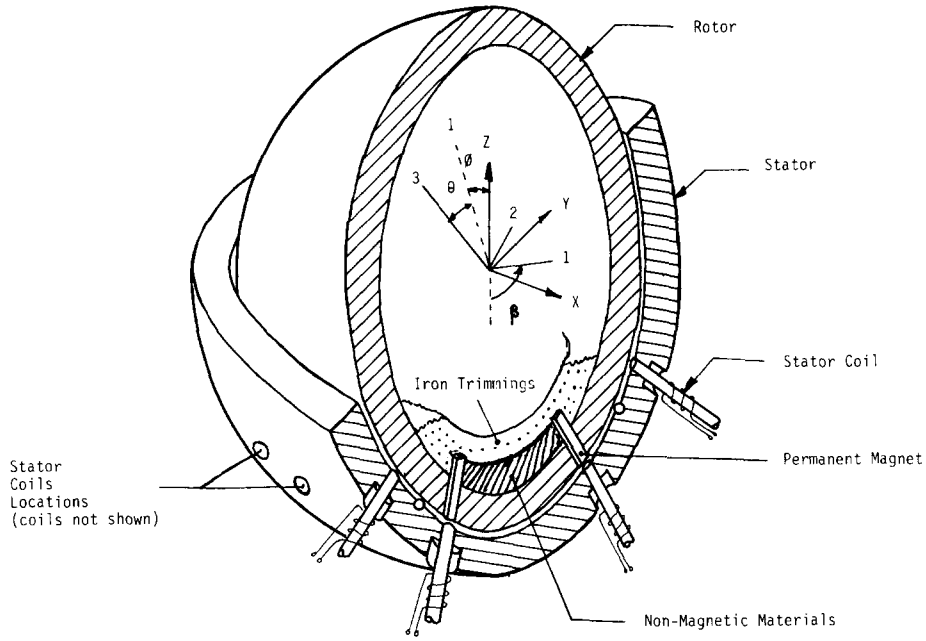

Fig. 1. Conceptual schematic of a spherical wrist motor.

It was chosen primarily because it is convenient to construct it in the laboratory and thus demonstrate concept feasibility. The motor consists of a hemispherical stator which houses the stator coils and a rotor which houses a pair of permanent magnets. The rotor is supported freely by means of gimbals. The spherical stepper motor operates on the principle of VR motor. The stator coils can be energized individually using the control circuitry. As a pair of the stator coils adjacent to the permanent magnets is energized so that a magnetic field and a corresponding flux are generated, the tangential components of the magnetic forces attract the adjacent magnets and hence exert a resultant torque on the rotor. Appropriate sequencing of high current pulses excites the stator coils and as a result, the rotor produces a movement in any direction desired. The maximum torque generated and the resolution obtainable depend primarily on the geometry, the arrangement of the coils, the number of magnets as well as the m.m.f. generated by the coils.

The principle of operation of the three DOF spherical stepper motor differs significantly from the single axis stepper motor. The primary difference is the required number of energized coils at any particular static orientation for mechanical stability and for three DOF motion control. As the conventional stepper motor is constrained physically to rotate about one axis, only one force is necessary to actuate or to lock the motion of the rotor in that direction. However, the spherical actuator has an infinite number of rotational axes and has three degrees of freedom. With only one energized coil, the permanent magnet, as a point on the rotor surface can be actuated

in any direction along the tangential inner surface of the stator and thus provide two degrees of freedom motion control on the tangent surface. To provide the third DOF motion control, which is the spin motion about an axis through the center of the rotor and the point of attraction, a second force must be generated by the attraction between an additional active coil and a second permanent magnet which generate an actuating torque perpendicular to the tangent surface. Hence, for stability of the rotor at a static position of for three DOF motion, two forces which are not colinear with the center of the rotor are necessary at any instant to provide motion control of the rotor.

The second difference stems from the fact that the maximum number of coils which can be evenly inscribed on a spherical surface is finite. The locations of the evenly spaced coils can be determined by building a polyhedron which is three dimensional solid with polygons as faces (sides). For equal spacing, regular congruent polygons such as equilateral triangles, square, or pentagons must be used. A point of a polyhedron makes up a convex polyhedral angle. Pythagoras and Plato [14] have shown that a complex polyhedral angle must be made up by at least three faces and must be less than 360° to form a closed polyhedron. Based on these principles, it can be shown that the maximum number of coils which can be evenly spaced on a sphere is 20 which is a number corresponding to the number of complex angles of a dodecuhedron.

The kinematic and dynamic equations for the spherical stepper motion are derived in the Appendix. The X–Y–Z Euler angles $q(\phi, \theta, \beta)$ are chosen to describe the orientation of the coordinate frame 123 with respect to the inertia frame, instead of the usual Z–Y–Z Euler angles which are indeterminate when the Z-axis and the 3-axis coincide. Unlike the single-axis motor, the dynamic equations of the three DOF spherical motor, as shown in the Appendix, are coupled, time-varying and nonlinear and thus the torques generated depend on the rotor orientation and the spacing of the stator coils in addition to the payload. However, due to its relatively simple ball-like rotor structure, the undesired cross-coupling and centrifugal components of the wrist rotor dynamics can be effectively eliminated if the unbalanced moment of inertia can be designed such that:

$$I_{ij} = 0, \quad i \neq j,$$

$$= I, \quad i = j.$$

Hence, with a low moment of inertia, I, the spherical stepper motor is essentially a low-inertia robotic wrist. This represents a significant advantage as compared to the wrist design with three-consecutive-rotational joints.

2.1. COIL ARRANGEMENT

More than 20 coils are typically required in order to achieve a high positional resolution. A scheme, therefore, was devised to space the coils on the lower hemisphere

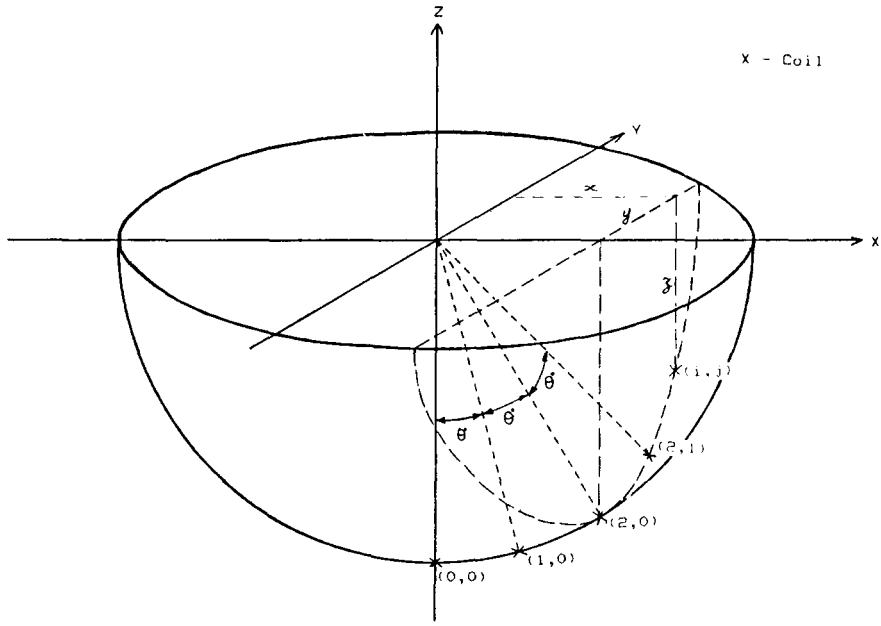

Fig. 2. Schematic illustrating coil arrangement.

of the stator as evenly as possible. The position of every coil is represented by the following mathematical relation as illustrated in Figure 2. The inner surface of the stator is described by the spherical surface ST, radius r, and the coil positions are represented by an array of points, CP. The spacing between the points is set by the angular parameter θ which is in degrees and is positive.

$$\text{ST} = \{(X, Y, Z): X^2 + Y^2 + Z^2 = r^2;\ Z \leqslant 0.0 \text{ and } (X, Y, Z) \in R^3,\ r \in R\},$$

$$\text{CP} = \{[(X, Y, Z), (i, j)]: (X, Y, Z) \in \text{ST and } (i, j) \in I\},$$

$$[(X, Y, Z), (i, j)] \in \text{CP}$$

iff

$$X = r \sin(i\theta)$$

and if $j = 0$ then

$$y = 0 \quad \text{and} \quad Z = -r \cos(i\theta)$$

or if $j \neq 0$, there exist $[(a, b, c), (i, j\text{-sgn}(j))] \in \text{CP}$ s.t.

$$(X, Y, Z) \cdot (a, b, c) = r^2 \cos\theta.$$

It has been shown that the least number of attractions to provide locking of the rotor is two. For a given pair of magnets, the above arrangement of stator coils determines the primary resolution, which is defined by the spacing of the coils.

Further improvement of resolution can be achieved by increasing the number of magnet pairs, modifying the radius of the rotor or microstepping control between adjacent coils. Without loss of generality, the rotor is assumed to have two permanent magnets in the following analysis.

2.2. TORQUE PREDICTION

The torque generated by the magnetic system is derived from the principle of conservation of energy, which yields:

$$\dot{E}_m(t) = \dot{E}_e(t) - \mathbf{T}(t) \cdot \boldsymbol{\omega}(t), \tag{1}$$

where $\dot{E}_m$ = time rate of increase in magnetic energy stored,
$\dot{E}_e$ = electrical power input = $\Sigma_{n=1}^{k} i(t) \cdot \dot{\lambda}(t)$
i_n = current through the nth excited coil,
λ_n = flux linkage through the nth excited coil,
$\mathbf{T}$ = resultant torque acting on the rotor, and
$\boldsymbol{\omega}$ = angular velocity of the rotor.

Since the magnetic energy is a function of the configuration of the magnetic system, i.e. the coil current, the relative position of the rotor, and all relevant functions will be expressed in terms of the Euler angle $q(\phi, \theta, \beta)$.

The torque components in the directions of $\mathrm{d}q(\phi, \theta, \beta)/\mathrm{d}t$ are found first and, then, resolved in the three orthogonal components in the 123 directions. The dot product of the torque $\mathbf{T}$ and the angular velocity $\boldsymbol{\omega}$ is:

$$\mathbf{T} \cdot \boldsymbol{\omega} = (T_\phi + S_\theta T_\beta)\dot{\phi} + T_\theta \dot{\theta} + (T_\beta + S_\theta T_\phi)\dot{\beta}, \tag{2}$$

where

$$\mathbf{T} = \mathbf{T}[T_\phi, T_\theta, T_\beta] \quad \text{and} \quad \boldsymbol{\omega} = \boldsymbol{\omega}[\omega_1, \omega_2, \omega_3].$$

The angular velocity can be related to the Euler angles and their time-derivatives as shown in Equation (A.2). The time derivatives of the energy terms, E_m and E_e, are partial differentials with respect to the Euler Angles, ϕ, θ, and β. With a constant current source for the stator coils, Equation (1) becomes

$$\left[T_\phi + T_\beta S_\theta + \frac{\partial E_m}{\partial \phi} - \sum_{n=1}^{k} \left(i_n \frac{\partial \lambda_n}{\partial \phi}\right)\right]\dot{\phi} + \left[T_\theta + \frac{\partial E_m}{\partial \theta} - \sum_{n=1}^{k} \left(i_n \frac{\partial \lambda_n}{\partial \theta}\right)\right]\dot{\theta} +$$

$$+ \left[T_\beta + T_\phi S_\theta + \frac{\partial E_m}{\partial \beta} - \sum_{n=1}^{k} \left(i_n \frac{\partial \lambda_n}{\partial \beta}\right)\right]\dot{\beta} = 0. \tag{3}$$

Since this equation is true for any $[\mathrm{d}q(\phi, \theta, \beta)/\mathrm{d}t]$, it holds only when the coefficients of the velocity term are zero. Under this condition, three linear simultaneous equations in the torque components are obtained. The three torque components were

solved for and are as follows

$$T_\phi = \frac{1}{C_\theta^2}\left[S_\theta \frac{\partial E_m}{\partial \beta} - \frac{\partial E_m}{\partial \phi} + \sum_{n=1}^{k} i_n \left(\frac{\partial}{\partial \phi} - S_\theta \frac{\partial}{\partial \beta}\right)\lambda_n\right], \tag{4}$$

$$T_\theta = \sum_{n=1}^{k}\left(i_n \frac{\partial \lambda_n}{\partial \theta}\right) - \frac{\partial E_m}{\partial \theta}, \tag{5}$$

$$T_\beta = \frac{1}{C_\theta^2}\left[S_\theta \frac{\partial E_m}{\partial \phi} - \frac{\partial E_m}{\partial \beta} + \sum_{n=1}^{k} i_n \left(\frac{\partial}{\partial \beta} - S_\theta \frac{\partial}{\partial \phi}\right)\lambda_n\right]. \tag{6}$$

After transformation, the torque can be expressed in terms of three orthogonal vector components in the direction of frame 123:

$$T_1 = T_\phi C_\theta C_\beta + T_\theta S_\beta, \tag{7}$$

$$T_2 = -T_\phi C_\theta S_\beta + T_\theta C_\beta, \tag{8}$$

$$T_3 = T_\phi S_\theta + T_\beta. \tag{9}$$

To determine the stored magnetic energy, a simplified model for the conceptual structure shown in Figure 3 is assumed in the following discussions in order to illustrate the design concept. In practice, the closed magnetic path can be realized by filling the rotor to a certain depth with iron trimmings, connecting the metallic cores of the coils by means of laminations, and allowing for a small stator coil spacing to ensure an overlapping area between the core and the magnet. As the permeability of the iron parts is generally large as compared to that of an air gap, the permeability of the iron parts in the system is assumed to be infinite. On the other hand, the

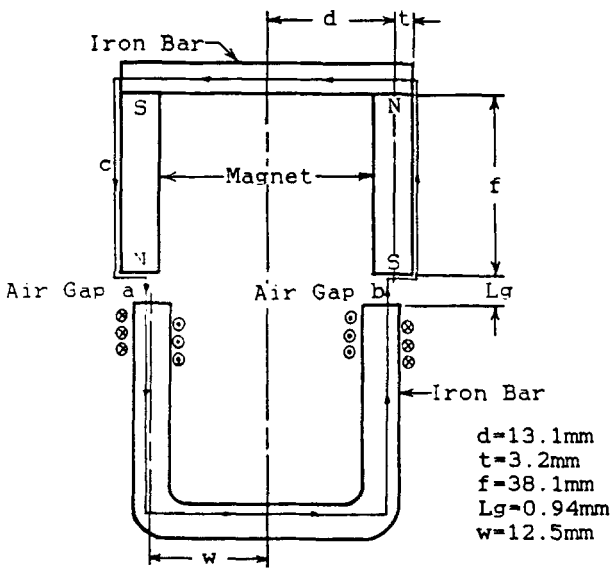

Fig. 3. Schematic of the magnetic system.

flux linkage surrounding the magnets cannot be ignored as the permeability of the magnets is of the same order as that of air. With these assumptions, the magnetic stored energy can be determined from an equivalent magnetic circuit which can be derived using Thevenin's Theorem. This yields:

$$E_m = \tfrac{1}{2}\Phi^2 R, \tag{10}$$

where Φ is the magnetic flux flow through the equivalent magnetic circuit with resultant reluctance, R. The refluctance is the reciprocal of the permeance which can be derived from the following equation:

$$P = \mu \int \frac{\mathrm{d}A}{L}, \tag{11}$$

where μ is the permeability and $\mathrm{d}A$ is a differential cross-section area of the flux tube as a function of tube length, L. The arc-straight line method as suggested in reference [15] was used to model the air gap permeance based on the assumed flux patterns which were detailed in [16], where the integration was performed numerically. The magnet flux can be obtained by dividing the total m.m.f. of the magnetic circuit, which can be derived from Maxwell's equation along a closed-path for specified magnetic properties, by the reluctance.

2.3. EXPERIMENTAL STATIC TORQUE PREDICTIONS

It is generally expected that the magnetization curve of the magnets is non-linear. Thus, an experimental prediction of the reluctance forces using a pair of Neodymium permanent magnets (6 mm × 6 mm × 38 mm) was performed on the system as shown in Figure 3. The magnetic flux density of the magnetic, B_m, is determined experimentally to be 0.7 Wb/m^2. The experimental data are displayed in Figure 4. The maximum force of 7 N is obtained with a current of 4 Amperes and a total of 600 turns on an iron bar of 1/4 inch diameter. Hence, with a spherical rotor of 125 mm diameter, a maximum restoring torque of 0.44 Nm may be obtained. Also, a maximum force of 3 N is observed with zero m.m.f. implying that a repulsive force in addition to the attractive force is necessary in switching the magnet from one coil to the other.

Although the theoretical data which are computed using a permeance-based model [15, 16] does not match the measured force exactly, they are in good qualitative agreement. In addition, the model gives a reasonably good prediction of the location of the peak. The force-separation curves predict the optimum spacing of 6 mm between the stator coils, which results in a maximum restoring torque to move the permanent magnet from one stator coil to another. Further increase of the spacing between stator coils may result in a nonrecoverable condition due to the decay of restoring force with distance.

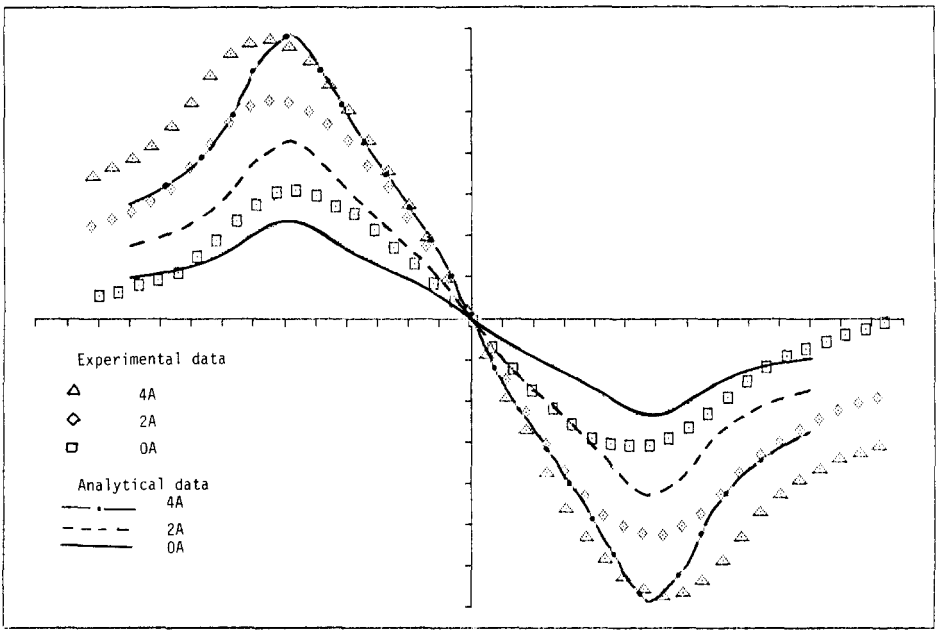

Fig. 4. Predicted reluctance force.

2.4. RESOLUTION

The primary resolution of the spherical stepper motor depends on the spacing of the stator coils. The resolution of the stepper motor can be improved effectively by (1) increasing the number of magnets and/or (2) microstepping control between the adjacent coils. The following discussion focuses on the first scheme whereas the second issue will be detailed in a forthcoming paper [17].

To facilitate the discussion, the definitions of phase and pole are introduced. A phase is defined as a set of coils which are turned on at the same time instance in order to actuate or control the rotor at a specified orientation. As it has been shown previously, since at least two attraction points are necessary for mechanical stability, the minimum number of coils per phase is two. A pole is defined as a set of permanent magnets which will be attracted by the active coils at a specified rotor orientation. Similarly, the minimum number of magnets per pole is two.

Hence, if there are N phases and one pole the rotor can be positioned at N specific orientations. To control the rotor orientation in-between the discrete N specified orientations, additional phases or poles can be added to the corresponding desired positions on the inner stator surface or on the rotor, respectively. The maximum number of desired discrete orientations is equal to the product of the number of the phase and that of the pole. To improve the resolution of motion in one particular direction by a factor of two, for a given phase, two poles are necessary for $2N$ desired

discrete orientations in that direction. If the resolution of motion in a second direction is to be improved by the same factor, the total number of desired discrete orientation is $2*(2N)$ or $4N$. In other words, three additional poles are required to improve the resolution by a factor of two in both directions. In general, it can be deduced that if the resolution of motion is to be improved by a factor of p times in q directions, (p^{q-1}) additional poles are required for a given number of phases.

3. Laboratory Prototype Development

A prototype which consists of a spherical stepper wrist motor, a digital controller and an analog excitation circuitry was constructed. The hybrid digital/analog scheme as shown in Figure 5 was developed in order to provide the appropriate sequencing and control functions of the spherical stepper wrist motor. The goals of the laboratory prototype were to demonstrate proof of concept feasibility, to serve as a testbed for the development of the excitation and control circuitry and to assist in achieving an optimum design.

3.1. PROTOTYPE WRIST MOTOR

The prototype wrist consists of a spherical rotor built from two hollow hemispheres, a hemispherical stator and a holding ring. All of these parts are machined out of Lexan material. The stator teeth on the prototype are # 10-32 machine screws wound with coils which are spaced according to the mathematical relationship outlined in Section 2.1. The coil separations on one quarter of the stator are listed in Table I. In the feasibility testing of the prototype, four coils and one magnet were installed as shown in the figure. Although the design described in this section addresses the case of a single permanent magnet–four stator coils with corresponding movement in the spherically mapped x–y coordinate system, the extension to a multiple permanent

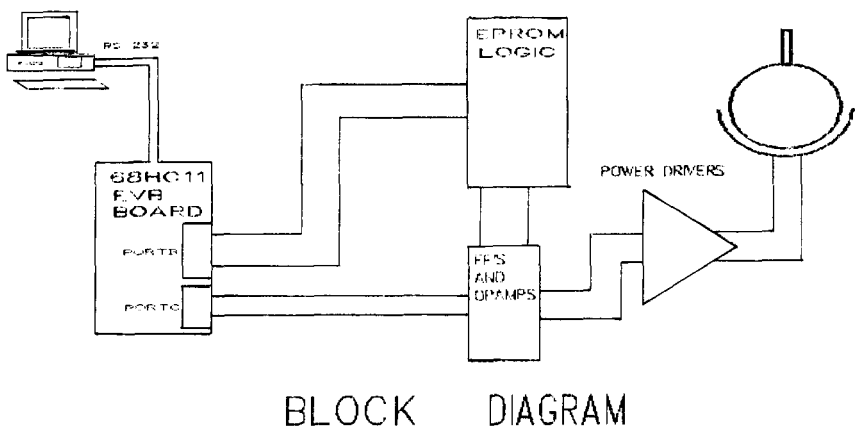

Fig. 5. Representation of the overall control and activation circuitry.

Table I. Coil separation table (Distance in mm)

(0,0)*	16.6	(1,0)	16.6	(2,0)	16.6	(3,0)	16.6	(4,0)	16.6	(5,0)
16.6		16.6		16.6		16.6		16.6		16.6
(0,1)	16.6	(1,1)	16.7	(2,1)	16.9	(3,1)	17.6	(4,1)	20.4	(5,1)
16.6		16.6		16.6		16.6		16.6		16.6
(0,2)	16.6	(1,2)	17.0	(2,2)	17.9	(3,2)	20.3	(4,2)		
16.6		16.6		16.6		16.6				
(0,3)	16.7	(1,3)	17.5	(2,3)	19.5	(3,3)				
16.6		16.6		16.6		16.6				
(0,4)	16.7	(1,4)	18.1	(2,4)	21.5	(3,4)				
16.6		16.6		16.6						
(0,5)	16.8	(1,5)	18.9	(2,5)						

*() indicates coil index (i, j).

magnet arrangement follows similar guidelines. Emphasis was placed on the design of the appropriate circuitry that would provide maximum flexibility in allowing the implementation of a variety of activation schemes and the determination of the sensitivity to wrist parameter changes. Clearly the goal here is to realize a laboratory prototype that will assist in achieving an optimum design.

3.2. DIGITAL SECTION

A two-level control scheme, coarse-fine motion, is proposed for a pre-planned trajectory. The first level is the open-loop position control of the rotor teeth (permanent magnets) based on the switching circuitry for a pre-planned trajectory. In the second level, accuracy and stability are such important issues that robust and fast convergent algorithms should be applied to fine-motion control in-between the decrete steps. This sections discusses the open-loop switching circuitry whereas the second level will be addressed in the forthcoming paper [17].

The digital control section consists of the following four parts:

(a) A *personal computer* is used as a host from which current level micro-controller code is downloaded to a Motorola 68HC11 board serially via an RS232 port. The PC is basically used to perform switching-sequence planning for a specified trajectory and as a system input/output device. Its function is to receive operator commands, determine the firing sequence and send their ASCII representation to the 68HC11. Finally, it receives and displays status messages consisting of echoing the stator movement to the screen.

(b) A *Motorola 68HC11 micro-controller* in conjunction with a Motorola EVB board is used to facilitate communication with the PC and to provide additional ports as control lines. The 68HC11 receives commands from the operator terminal and performs the functions decoded. Current options are: move up, move down, move left, move right, and teach mode. Teach mode allows the user to program stator positions that are to be moved repeatedly. Stator coils are actuated only if the 68HC11 determines that the position is valid. The program converts the command into a stator address that is sent to the EPROM decode block via the PORT C bus lines.

(c) An *EPROM Decode Block* consists of a bank of six 2764 EPROMS loaded with stator firing positions to facilitate design flexibility. Each individual data line of this 2764's is used to control a specific stator coil. The current hardware configuration can control up to 48 stator coils. Changes in the number of coils to be controlled, the number of coils fired at a time, and the firing sequence can be handled by simply reprogramming the EPROM.

(d) A *Repulsion Flip-FLop Block*–consisting of a 74L73 flip-flop with clear. Since a repulsion force is required whenever a stator coil is deactivated, there is one repulsion flip-flop circuitry allows control of three different logic states, attraction, repulsion and idle with only one control line and a global clear line for all flip-flops. This method thus allows control of N stator coils with $N + 1$ control lines.

The development software uses a noninteractive version of the 68HC11 assembly code to keep complexity at a minimum. It allows for switching between different hardware configurations along with different firing sequences. Figure 6 depicts the details of the microprocessor, EPROM and flip-flop connections. Figure 7 indicates the timing diagrams for the control signals.

3.3. ANALOG EXCITATION CIRCUITRY

The analog section consists of the following three main parts:

An *operational amplifier stage* connects directly to the outputs of the repulsion flip-flops and the EPROM. It generates the required positive and negative voltage levels for the stator attraction and repulsion modes, respectively. The square wave output is connected directly to the power transition stage.

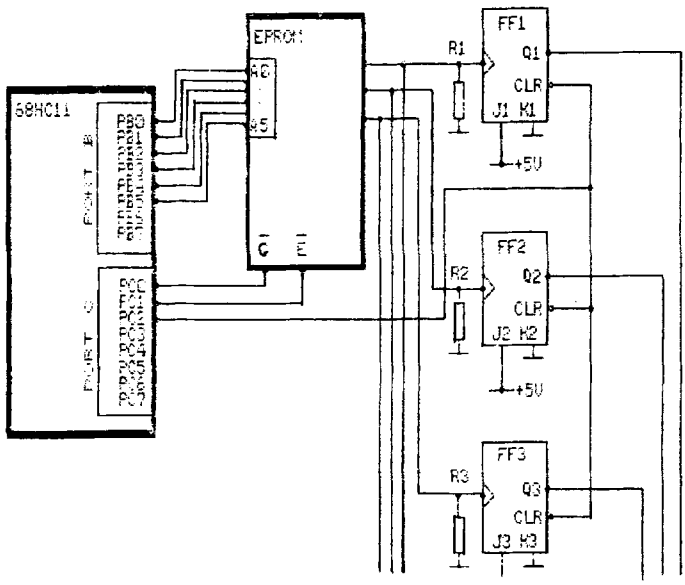

Fig. 6. Microprocessor, EPROM and flip-flop connection.

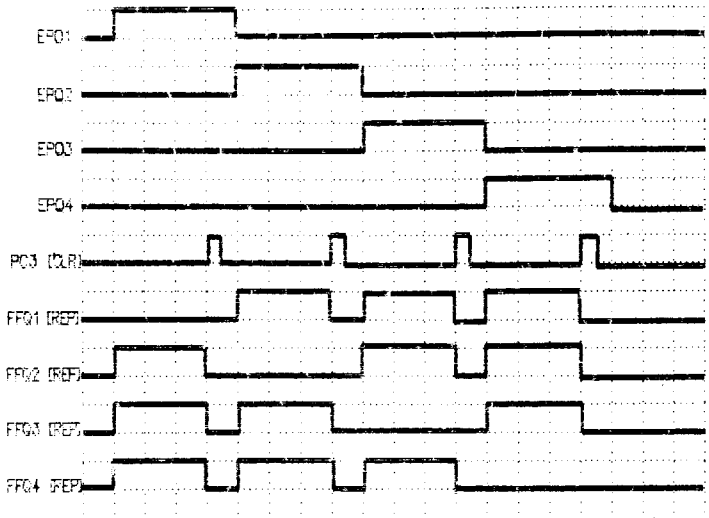

Fig. 7. Timing diagram for the signals produced by the 68HC11 board, FF's and the EPROM.

Bipolar Power Transistors provide current to the stator coils of up to two amperes when connected directly to the op amp output. Each stator coil employs two such transistors, one generating the positive current associated with attraction forces and the second generating the negative current associated with repulsion. The two transistors are configured in a push-pull format, with the stator coils connected as the load.

Stator coils are energized by the power transistor outputs and controlled via the EPROM control lines. Each stator coil has currently three stable current states: $+2$ amps, -2 amps and zero amps. Figure 8 shows the op-amp and power transistor connections. Figure 9 indicates the timing diagrams for the control and actuation signals.

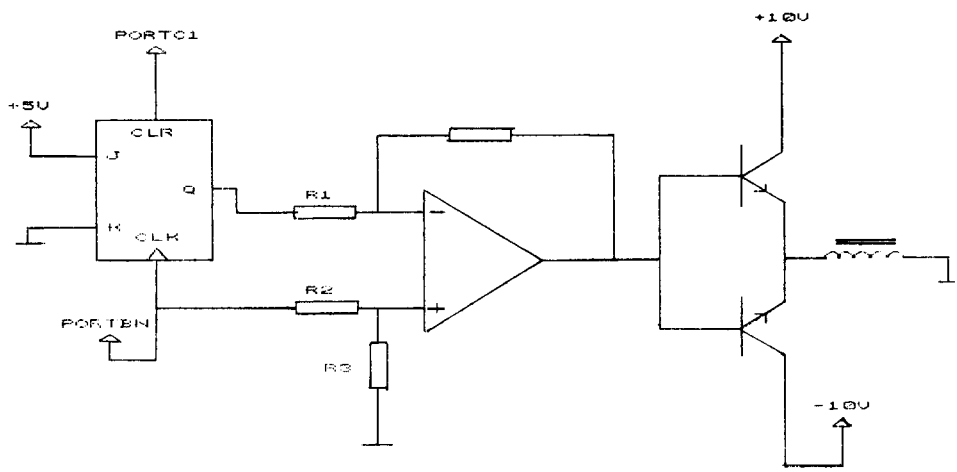

Fig. 8. Op-Amp and power transistor connections.

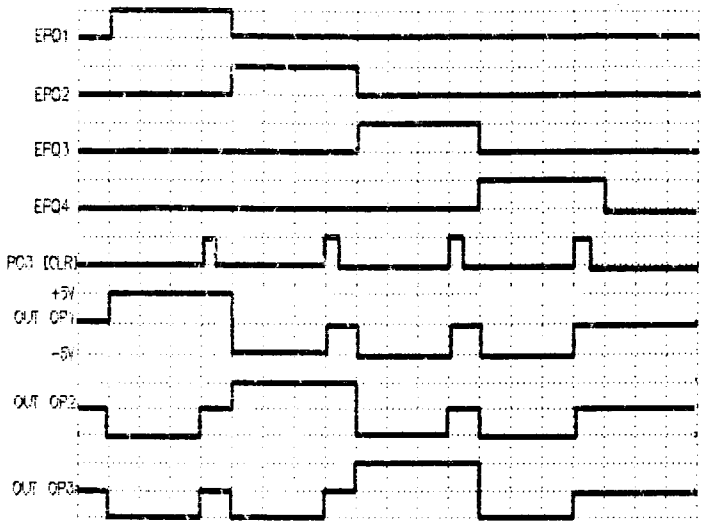

Fig. 9. Timing diagram for operation amplifier outputs.

3.4. LABORATORY TESTING

The hybrid digital/analog control and excitation circuitry has been tested on a laboratory prototype wrist motor, which is displayed in Figure 10. A number of different switching schemes to position the magnet at four specified coil locations in sequence have been tested. In the first scheme, three of the four coils were excited to generate the repulsive forces and the fourth coil was excited to generate an attractive

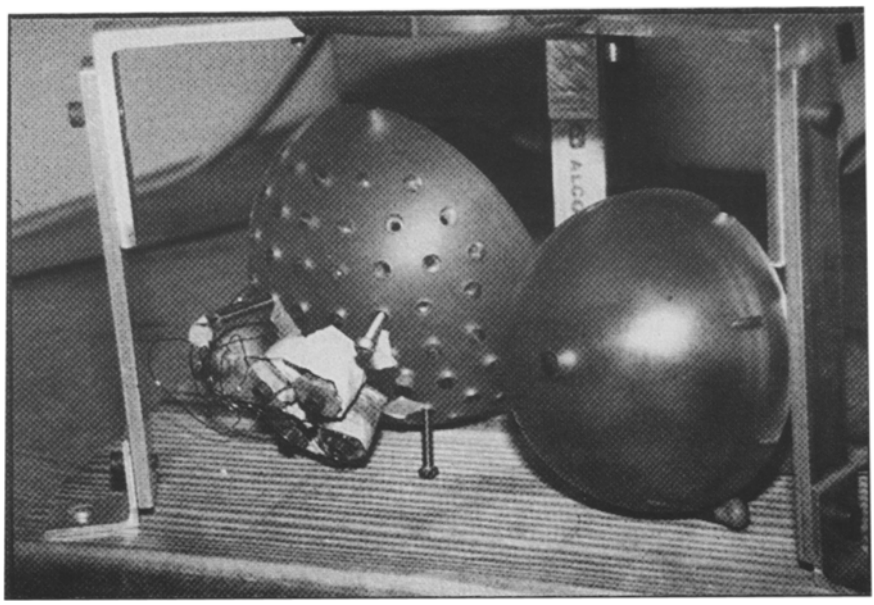

Fig. 10. Laboratory prototype wrist motor.

force in sequence. The result of the laboratory testing has indicated that a stable orientation control using variable switching sequence can be obtained as expected. In the second scheme where only three of the four coils were excited to produce the repulsive forces and the fourth coil was left unattended in the switching sequence, it was interesting to observe that a stable switching sequence can be maintained due to the attraction of the permanent magnet. In the third scheme where only one of the four coils was excited and the other three coils were left unattended, the motion of the rotor was unpredictable. The result of the third scheme has confirmed the need of multiple firing due to the attraction of the magnet and the relatively large space between the adjacent coils.

4. Conclusions

The design concept of a new electromechanical spherical stepper wrist motor capable of three DOF motion in a single joint is presented. Although the wrist motor is developed on the basis of a VR stepper motor principle, its operation significantly differs from that of a conventional single-axis VR stepper motor.

Along with the presentation of the kinematic and dynamic relationships, an analysis of torque prediction has been performed. Preliminary experimental torque predictions suggest that a maximum of 0.44 Nm restoring torque can be obtained with a pair of Neodymium permanent magnets (6 mm $\times$ 6 mm $\times$ 38 mm) on a rotor of 125 mm diameter although significant increase of restoring torque can be expected by increasing the permanent magnet pairs and/or the m.m.f. through the coils. However, the realization of an optimum design for a spherical stepper wrist motor is far from complete. Further work on prototype development, computer simulation and experimental verification of torque and resolution predictions are currently underway.

A laboratory prototype hybrid digital/analog control circuitry has been developed to assist in achieving an optimum design. The laboratory prototype performs well-showing proof of concept feasibility. Work underway is addressing the issues of a multiple permanent magnet arrangement in order to achieve full three DOF motion and a variable current source for stator coil actuation and control purposes. Associated research tasks are exploring means for detecting the position of the rotor.

Appendix:

KINEMATIC AND DYNAMIC MODEL

As shown in Figure 1, an inertia coordinate frame, designated as XYZ, is fixed at the center of the stator with its Z axis pointing towards the open-end of the stator hemisphere. Similarly, a body coordinate frame 123 is assigned to the center of the rotor, with its 3-axis pointing towards the center of the end-effector platform. The unit vectors along the (X, Y, Z) and (1, 2, 3) coordinates are designated as (I, J, K) and (i, j, k), respectively.

A.1. KINEMATIC RELATIONSHIP

The X–Y–Z Euler angles $q(\phi, \theta, \beta)$ are chosen to describe the orientation of the coordinate frame 123 with respect to the inertia frame, instead of the usual Z–Y–Z Euler angles because the Z–Y–Z Euler angles are indeterminate when the Z-axis and 3-axis coincide. The homogenous transformation $[T]$ between the two coordinate system is

$$[\mathbf{i}, \mathbf{j}, \mathbf{k}]^T = [T]\,[\mathbf{I}, \mathbf{J}, \mathbf{K}]^T, \tag{A.1}$$

where

$$[T] = \begin{bmatrix} C_\theta C_\beta & S_\theta S_\phi C_\beta + S_\phi C_\phi & -S_\theta C_\phi C_\beta + S_\phi S_\beta \\ -C_\theta S_\beta & -S_\theta C_\phi C_\beta + C_\phi S_\phi & S_\phi C_\theta C_\psi + S_\phi C_\beta \\ S_\theta & -S_\phi C_\theta & C_\theta C_\phi \end{bmatrix},$$

where the subscripts of C and S are the angles of cosines and sines, respectively. The Euler angle $q(\phi, \theta, \beta)$ is the general coordinate of the rotor. The angular velocity and acceleration of the rotor relative to the inertia frame can be described by the first and second derivatives of the $q(\phi, \theta, \beta)$, respectively. However, it will be more convenient to express the terms in vector form, with respect to the rotating frame, as far as the dynamics are concerned. If the angular velocity of the body coordinate, ω is

$$\boldsymbol{\omega} = \omega_1 i + \omega_2 j + \omega_3 k \tag{A.2}$$

where $\omega_1 = \dot{\phi} C_\phi C_\beta + \dot{\theta} S_\beta,$
$\omega_2 = -\dot{\phi} C_\theta S_\beta + \dot{\theta} C_\beta,$
$\omega_3 = \dot{\phi} S_\theta + \dot{\beta}.$

The corresponding angular acceleration $\mathrm{d}\omega/\mathrm{d}t$ is

$$\frac{\mathrm{d}\boldsymbol{\omega}}{\mathrm{d}t} = \dot{\omega}_1 \mathbf{i} + \dot{\omega}_2 \mathbf{j} + \dot{\omega}_3 \mathbf{k} \tag{A.3}$$

where $\dot{\omega}_1 = \ddot{\phi} C_\theta C_\beta + \theta S_\beta + \dot{\theta}\dot{\beta} C_\beta + \dot{\phi}\dot{\theta} S_\theta C_\beta - \dot{\phi}\dot{\beta} C_\theta S_\beta,$
$\dot{\omega}_2 = -\ddot{\phi} C_\theta S_\beta + \ddot{\theta} C_\beta - \dot{\theta}\dot{\beta} S_\theta S_\beta + \dot{\phi}\dot{\theta} S_\theta S_\beta - \dot{\theta}\dot{\beta} C_\theta C_\beta,$
$\dot{\omega}_3 = \ddot{\beta} + \ddot{\phi} S_\beta + \dot{\phi}\dot{\theta} C_\theta.$

When the forward dynamics problem is of interest, i.e. prediction of the rotor orientation $q(\phi, \theta, \beta)$ for a given external moment applied on the rotor, the conversion from the vector components to the Euler angle $q(\phi, \theta, \beta)$ is desired. The conversion equations have been derived as follow:

$$\begin{aligned} \dot{\phi} &= \frac{1}{C_\theta}(\omega_1 C_\beta + \omega_2 S_\beta), \\ \dot{\theta} &= \omega_1 S_\beta - \omega_2 C_\beta, \\ \dot{\beta} &= \omega_3 - \tan\theta\,(\omega_1 C_\beta - \omega_2 S_\beta). \end{aligned} \tag{A.4}$$

A.2. DYNAMIC MODEL

Unlike a single axis motor, the dynamic equations of the three DOF spherical motor are coupled and nonlinear. The dynamics equations are derived from the principle of conservation of angular momentum. If the design of the rotor is such that the 1, 2, and 3 coordinate axes are the principle axes, i.e. $I_{12} = I_{23} = I_{13} = 0$, the equations will be reduced to

$$\begin{aligned} \mathbf{M}_1 &= I_1\dot{\omega}_1 + (I_3 - I_2)\,\omega_2\omega_3, \\ \mathbf{M}_2 &= I_2\dot{\omega}_2 + (I_1 - I_3)\,\omega_1\omega_3, \\ \mathbf{M}_3 &= I_3\dot{\omega}_3 + (I_2 - I_1)\,\omega_2\omega_1 \end{aligned} \tag{A.5}$$

where $\mathbf{M} = [M_1 M_2 M_3]^T$ is the external moment applied on the rotor about its center of gravity and can be expressed as

$$\mathbf{M} = \mathbf{T}(\mathbf{q}, \dot{\mathbf{q}}, \ddot{\mathbf{q}}) + \mathbf{F}(\dot{\mathbf{q}}) + \mathbf{M}_l(\mathbf{q}),$$

where $\mathbf{T}$ is the actuating torque vector generated by the magnetic system $\mathbf{F}$ and $\mathbf{M}_l$ are the friction and load torque vectors, respectively. Rearranging Equation (A.5), as a system of first order differential equations results in:

$$\begin{aligned} \dot{\omega}_1 &= \frac{1}{I_1}[(I_2 - I_3)\,\omega_2\omega_3 + M_1], \\ \dot{\omega}_2 &= \frac{1}{I_2}[(I_3 - I_1)\,\omega_1\omega_3 + M_2], \\ \dot{\omega}_3 &= \frac{1}{I_3}[(I_1 - I_2)\,\omega_2\omega_1 + M_3]. \end{aligned} \tag{A.6}$$

Whereas Equations (A.2), (A.3) and (A.5) determine the actuating torque required given the orientation trajectories, Equations (A.4) and (A.6) together form a state space representation of the forward dynamics. The state variables are the Euler angles $q(\phi, \theta, \beta)$ and the angular velocity, with respect to frame 123, ω and the input is the external moment $\mathbf{M}$.

Acknowledgement

This research is supported by the General Research Fund of the School of Mechanical Engineering at Georgia Tech. Partial support by the Computer Integrated Manufacturing System (CIMS) Program at Georgia Tech is appreciated.

Reference

1. Asada, H. and Cro-Granlto, J.A., Kinematic and static characterization of wrist joints and their optimal design, *Proc. 1985 IEEE Int. Conf. on Robotics and Automation.*
2. Paul, R.P. and Stevenson, C.N., Kinematics of robots wrist, *Int. J. Robotics Res.* **2** (1983) 31–38.

3. Pieper, D.L., The kinematics of manipulators under computer control, PhD Thesis, Dept. Computer Science, Stanford University, 1968.
4. Bennett, A mechanical wrist for a robot arm, BS Thesis, MIT, 1968.
5. Rosheim, M.E., Robot wrist actuators, *Robotics Age*, Nov/Dec 1982.
6. Vachtsevanos, G.J., Davey K., and Lee, K., Development of a novel intelligent robotic manipulator, *Control Systems Magazine*, June 1987.
7. William, F., Laithwaite, E., and Piggot, L., Brushless variable-speed induction motors, *Proc. IEEE*, No. 2097U, pp. 102–118, June 1956.
8. Williams, F., Laithwaite, E., and Eastham, G.F., Development of design of spherical induction motors, *Proc. IEEE*, No. 3036U, pp. 471–484, December 1959.
9. Laithwaite, E., Design of spherical motors, *Electrical Times* **9**, 921–925 (1960).
10. Laing, I. and Laing, N., Patent U.S. 4352646, Rotodynamic pump with spherical motor, 5 October 1982.
11. Lebedev, A. and Shinyev, P., Moments acting in a spherical rotor in a magnetic suspension, *Priborostroegie* 16: 5, 85–88 (1973).
12. Izv Vyssh Uchebn Zaved, Electromagnetic processes in an asynchronous motor with a spherical hollow rotor, *Electromekh*, No. 11, 1231–1239, Nov. 1976.
13. Devay, K. and Vachtsevanos, G. The analysis of fields and torques in a spherical induction motor, *IEEE Trans. Mag.*, March 1987.
14. Smith, D.E., *Essentials of Plane and Solid Geometry*, Wentworth-Smith Mathematical Series, 1923.
15. Chai, H.D., Permeance model and reluctance force between toothed structures, *Theory and Applications of Step Motor* (ed. B.C. Kuo) West Publishing Co., 1973.
16. Kwan, C., An investigation of a spherical robot wrist actuator, MS Thesis (Mechanical Engineering), Georgia Institute of Technology, 1987.
17. Lee, K-M. and Arjunan, S., Force/torque sensing and micro-motion manipulation of a spherical stepping wrist motor, *Proc. 1988 Amer. Control Conf., Atlanta, Georgia.*